Journal of Power Sources 271 (2014) 97–103

Contents lists available at ScienceDirect

Journal of Power Sources

journal homepage: www.elsevier.com/locate/jpowsour

Differentiating allotropic $LiCoO_2/Li_2Co_2O_4$: A structural and electrochemical study

Yongchun Kan [a, b], Yuan Hu [a], Yang Ren [c], Javier Bareño [b], Ira Bloom [b], Yang-Kook Sun [d], Khalil Amine [b], Zonghai Chen [b, *]

[a] State Key Laboratory of Fire Science, University of Science and Technology of China, Hefei, Anhui 230026, PR China
[b] Chemical Sciences and Engineering Division, Argonne National Laboratory, Lemont, IL 60439, USA
[c] X-ray Science Division, Advanced Photon Source, Argonne National Laboratory, Lemont, IL 60439, USA
[d] Department of WCU Energy Engineering, Department of Chemical Engineering, Hanyang University, Seoul 133-791, South Korea

HIGHLIGHTS

- Allotropic $Li_2Co_2O_4/LiCoO_2$ were characterized using high resolution X-ray diffraction.
- Interexchange between Li and Co in octahedral sites occurs at a high temperature.
- A strained spinel phase between $LiCoO_2$ and $Li_2Co_2O_4$ is reported for the first time.

GRAPHICAL ABSTRACT

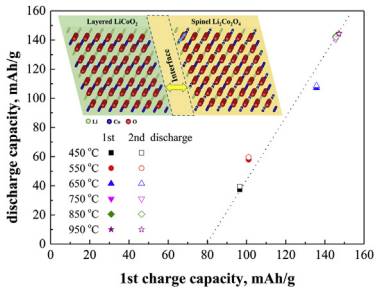

ARTICLE INFO

Article history:
Received 27 June 2014
Accepted 28 July 2014
Available online 6 August 2014

Keywords:
Allotropic structure
Lithium cobalt oxide
Structure property relationship
Cation mixing
Lithium battery

ABSTRACT

In situ high-energy X-ray diffraction was carried out to investigate the structural transformation of lithium cobalt oxides during the solid-state synthesis. Two allotropic phases were observed during the synthesis process; $Li_2Co_2O_4$ with a spinel structure was formed within the temperature window between 450 °C and 650 °C, beyond which $Li_2Co_2O_4$ was converted to its hexagonal counterpart, layered $LiCoO_2$, through a cation exchange between Li and Co. In electrochemical tests, the $Li_2Co_2O_4$ was estimated to have a very low reversible capacity, ~20 mAh g^{-1}, and a high initial irreversible capacity loss of about 80 mAh g^{-1}. An interfacial phase between layered $LiCoO_2$ domain and spinel $Li_2Co_2O_4$ domain was also identified by *ex situ* high-resolution X-ray diffraction.

1. Introduction

Allotropic compounds are generally considered a class of chemicals with identical nominal chemical formula, but with substantial differences in their chemical and/or physical properties. Diamond and graphite are a pair of typical allotropic compounds; the former is a super hard insulator while the latter is a soft electronic conductor. Allotropic structures are also widely found in inorganic oxides like PbO [1,2], TiO_2 [3–7], MnO_2 [8–12], and many others [13]. The allotropic structure has been a major barrier to establish the structure-property relationship of functional materials. Advanced structural characterization tools, like the *in situ* synchrotron probes used in this study, can provide valuable new insight for understanding and designing complex functional materials.

For instance, lithium cobalt oxide ($LiCoO_2$) has been the dominant cathode material for state-of-the-art lithium-ion batteries

* Corresponding author.
E-mail address: zonghai.chen@anl.gov (Z. Chen).

http://dx.doi.org/10.1016/j.jpowsour.2014.07.178
0378-7753/

since the early 1990s. This material is widely referred to as a "layered" material with a hexagonal structure in space group R-3m (166). What is not well known is its allotropic counterpart, spinel $Li_2Co_2O_4$, which is formed by a low-temperature synthesis. The difficulty in differentiating this pair of allotropic compounds lies in their similar scattering structure factor, making it difficult to identify $Li_2Co_2O_4$ by regular X-ray diffraction techniques. However, owing to the recent development of high-quality X-ray sources from synchrotrons [14], neutron sources [15], and high-resolution transmission electron microscopes [16–18], the structural difference between $Li_2Co_2O_4$ and $LiCoO_2$ can now be easily distinguished. Using neutron diffraction, Thackeray et al. [15] revealed the doping of Co atoms in lithium layers of $LiCoO_2$ when annealed at 400 °C. Rietveld refinement suggested a small degree of Li–Co intermixing (~6%) in samples sintered at low temperatures. Using *in situ* high-energy X-ray diffraction (HEXRD), Wicker et al. [14] tracked the structural evolution during the solid-state synthesis of $LiCoO_2$. They reported that the layered component, $LiCoO_2$, dominated the whole synthesis process, while only a small fraction of $Li_2Co_2O_4$ was observed at low temperature region. [14] In this work, we employed both *in situ* HEXRD and *ex situ* high-resolution X-ray diffraction (HRXRD) for a careful characterization of the $Li_2Co_2O_4$–$LiCoO_2$ system.

2. Experimental

2.1. Solid-state synthesis of cathode materials

Co_3O_4 and Li_2CO_3 with a molar ratio of 2:3.15 were mechanically mixed for 48 h. 5% excess lithium was added to compensate potential lithium loss during synthesis. Separate batches of the mixed powder were then heated at a constant rate of 5 °C min^{-1} in air to selected temperatures between 450 °C and 950 °C. The samples were then annealed at the selected temperatures for 16 h before being naturally cooled to the room temperature (RT).

2.2. In situ HEXRD

The powder mixture of Co_3O_4 and Li_2CO_3 was compressed into a pellet of about 2-mm in thickness. The pellet was then vertically placed in a programmable furnace (Linkam TS 1500) with the X-ray beam aimed at the center of the pellet. The sample was then heated from RT to 1050 °C with a constant heating rate of 1 °C min^{-1}. The *in situ* HEXRD experiment was carried out at sector 11-ID-C of the Advanced Photon Source (APS) at Argonne National Laboratory. The wavelength of the X-ray beam was pre-fixed at 0.10804 Å. During the *in situ* solid-state synthesis, a 2D X-ray detector was used to collect the XRD patterns at a rate of one spectrum per minute. The details of the experimental setup can be found in our previous report [19].

2.3. Ex situ HRXRD

The HRXRD patterns of cathode samples synthesized at various temperatures were collected at sector 11-BM of the APS. The wavelength of the X-ray beam used was 0.413326 Å.

2.4. Electrochemical characterization

The electrochemical performance of the cathode powders was tested in 2032 coin cells using a lithium foil as the anode. The cathode was fabricated with a mixture of cathode powder (80 wt %), Super P (10 wt%), and polyvinylidene fluoride (PVDF) (10 wt%) in *N*-methyl-2-pyrrolidone (NMP). The slurry was coated onto the aluminum foil and dried in a vacuum oven at 75 °C. The electrolyte was 1.2 M $LiPF_6$ in a mixture solvent of ethylene carbonate (EC) and ethyl methyl carbonate (EMC) with a mass ratio of 3:7. The half cells were charged/discharged between 3.0 V and 4.2 V at a constant current of 0.08 mA (C/10) at the room temperature.

3. Results and discussion

Fig. 1 shows the evolution of HEXRD profiles during the solid-state synthesis of $LiCoO_2$ using Co_3O_4 and Li_2CO_3 as the starting materials. During the *in situ* experiment, the starting materials were heated from the room temperature to 1050 °C with a constant rate of 1 °C min^{-1}. The characteristic diffraction peak positions for both Co_3O_4 (spinel, PDF card # 74–2120) and Li_2CO_3 (PDF card # 72–1216) are labeled at the bottom of Fig. 1. Thermal expansion of the lattice was observed, and the continuous shift of the diffraction peaks toward smaller 2θ values was observed up to 400 °C, beyond which the peak intensity for both Co_3O_4 and Li_2CO_3 decreased quickly. To further analyze the reaction between Co_3O_4 and Li_2CO_3, we used the peak area of the (110) peak for Li_2CO_3 ($2\theta = 1.49°$) to estimate the relative content of Li_2CO_3 during the solid-state reaction and the (422) peak for Co_3O_4 ($2\theta = 3.78°$) to estimate the Co_3O_4 content. Fig. 2a shows the evolution of peak areas as a function of the temperature. From RT to 400 °C, the peak area remained stable for Li_2CO_3 but slowly decreased for Co_3O_4. It is speculated that this change is related to the loss of moisture from Co_3O_4. Above 400 °C, the peak areas for both Li_2CO_3 and Co_3O_4 dropped dramatically at roughly the same rate. The strong correlation between the two starting materials is also illustrated in Fig. 2b, which indicates a strong linear relationship between Li_2CO_3 and Co_3O_4 content. This suggests that the solid-state reaction is a one-step reaction:

$$2/3\,Co_3O_4 + Li_2CO_3 + 1/2O_2 \rightarrow (1-x)\,Li_2Co_2O_4 + 2x\,LiCoO_2 + CO_2 \quad (1)$$

In the above reaction, the products of layered $LiCoO_2$ and spinel $Li_2Co_2O_4$ were identified from the *in situ* HEXRD data. Fig. 1 clearly shows the emergence of a new set of diffraction peaks when the temperature is above 400 °C. At the plotting scale of Fig. 1, the new peaks could be assigned to layered $LiCoO_2$ (R-3m, space group 166). However, the zoom-in view of the data between 3.9° and 4.05° in Fig. 3a shows that the new peaks were dominated by the spinel $Li_2Co_2O_4$ (F d-3m, space group 227). This figure clearly shows three characteristic diffraction peaks: the

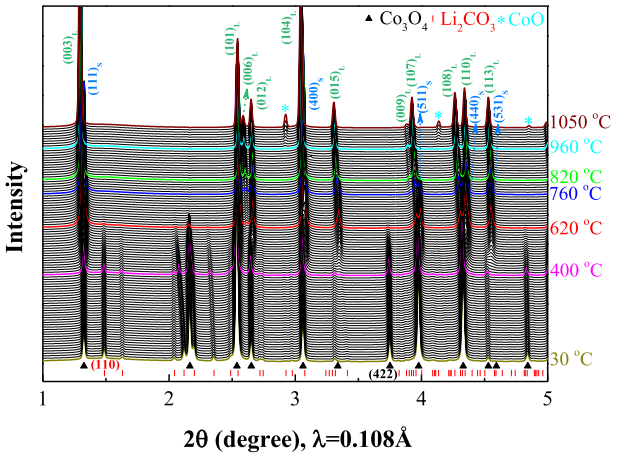

Fig. 1. HEXRD patterns during the solid-state synthesis of $LiCoO_2$ using Co_3O_4 and $LiCO_3$ as the starting materials.

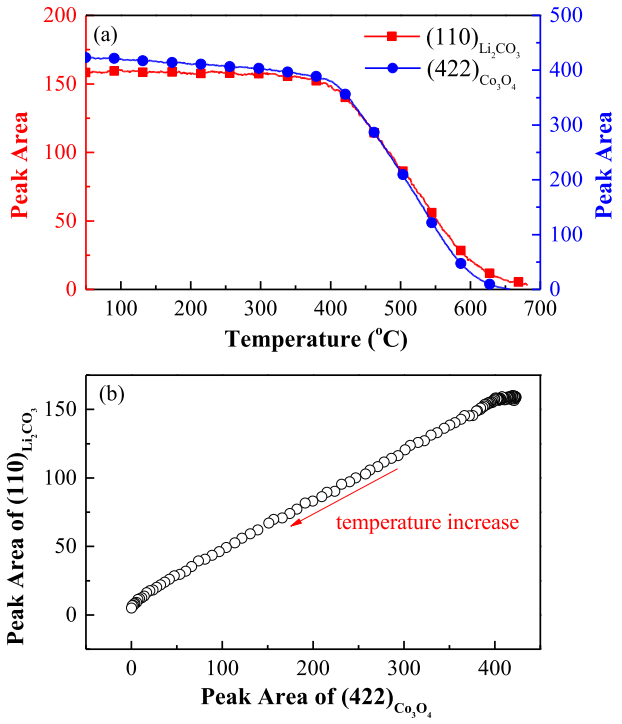

Fig. 2. Peak area for (110) peak of Li_2CO_3 and (422) peak of Co_3O_4 during solid-state reaction.

(511) peak for Co_3O_4 at the bottom; the $(511)_S$ peak for $Li_2Co_2O_4$ at the right, between 620 °C and 760 °C; and the characteristic $(107)_L$ peak for layered $LiCoO_2$ at the left. Fig. 3b shows that, within the temperature window between 620 °C and 760 °C, the $(107)_L$ and $(551)_S$ peaks are well separated from each other. The initial decrease in the peak intensity of $(107)_L$ is an artifact of the residual Co_3O_4 whose (551) peak overlaps with the $(107)_L$ peak. Other than that, the content of $LiCoO_2$ increases while that of $Li_2Co_2O_4$ decreases steadily with the heating temperature. This indicates that $Li_2Co_2O_4$ was the dominant product when the temperature was below 620 °C, beyond which $Li_2Co_2O_4$ converted to layered $LiCoO_2$. Fig. 3a shows that this conversion process finished at about 820 °C. The formed $LiCoO_2$ crystallized at a temperature above 820 °C, as indicated by the sharpening of the $(107)_L$ peak in Fig. 3a.

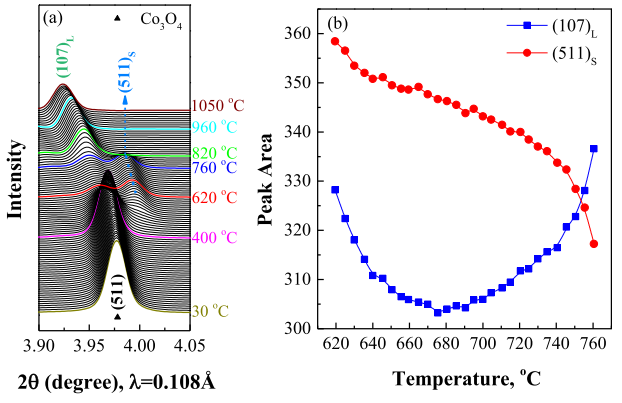

Fig. 3. (a) Zoomed view of HEXRD pattern within the 2θ range of 3.90° and 4.05°, and (b) the variation of peak area for (107) peak for layered $LiCoO_2$ and (551) peak for spinel $Li_2Co_2O_4$ as functions of the temperature.

When the sample was heated to a temperature beyond 960 °C, $LiCoO_2$ was partially decomposed into CoO (see Fig. 1) by losing both Li_2O and O_2. During the cooling process, CoO was converted back to the stable form Co_3O_4 (XRD data during the cooling process are not shown). As a precaution, the annealing temperature for the *ex situ* syntheses was limited to 950 °C.

The above results were obtained during a dynamic heating process with continuously changing temperature. It is of interest to determine whether the same reaction mechanism can be applied to steady-state synthesis. The *ex situ* experiments were thus carried out by annealing the cathode materials for 16 h at temperatures ranging from 450 °C to 950 °C. Fig. 4 shows the normalized HRXRD patterns of the samples annealed at these temperatures. Note that the wavelength of the HRXRD was 0.413 Å, which is much longer than that for HEXRD. It is common that the peak intensity increased rapidly with the annealing temperature because of the increase in crystallinity. It is of our interest to determine the relationship between different phases. Hence, the HRXRD patterns were normalized by rescaling the $(003)_L$ peak at 5.05°, for layered $LiCoO_2$, to unity (see Fig. 4). One can see that the peak width of the $(003)_L$ decreases steadily with the annealing temperature, but the peak position remains constant. More importantly, a big broad peak, which can be assigned to the $(111)_S$ peak for spinel $Li_2Co_2O_4$, appears at a slightly higher 2θ value, about 5.13°. Fig. 4 indicates that the spinel form $Li_2Co_2O_4$ was the major product when the annealing temperature is below 550 °C. This finding is not consistent with the report of Wicker and Walker [14] that the content of $Li_2Co_2O_4$ is low throughout the whole synthesis process. Fig. 4 also shows that the $Li_2Co_2O_4$ content decreases rapidly with the annealing temperature. At annealing temperature above 750 °C, the $(111)_S$ peak for $Li_2Co_2O_4$ completely disappeared from the HRXRD patterns in Fig. 4. This finding agrees with the *in situ* experiment, except that the finishing temperature for the conversion was higher for the *in situ* experiment.

Rietveld refinement was also carried out to fit the HRXRD data for the samples annealed at different temperatures. A two-phase model, involving layered $LiCoO_2$ and spinel $Li_2Co_2O_4$, was used to fit the data for samples annealed at 450 °C, 550 °C, and 650 °C. For annealing temperature higher than 650 °C, a single-phase model, layered $LiCoO_2$, was used. Table 1 shows the cell parameters obtained from the Rietveld refinement. The *a* and *b* values of layered $LiCoO_2$ slightly decrease (~0.04%) with the annealing temperature, while the *c* values increase slightly (~0.1%). Since the

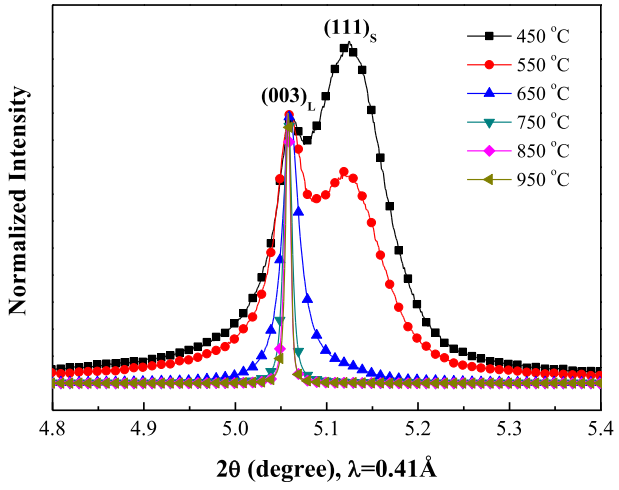

Fig. 4. Normalized HRXRD patterns of samples annealed at different temperatures showing the coexistence of $Li_2Co_2O_4$ and $LiCoO_2$ at a low temperature.

Table 1
Rietveld refinement for HRXRD data[a].

T, °C	$LiCoO_2$		$Li_2Co_2O_4$	wRp	CHI**2
	$a = b$	c	$a = b = c$		
450	2.8175(4)	14.040(6)	7.9982(4)	0.092	3.50
550	2.8163(9)	14.046(1)	7.9980(2)	0.111	4.59
650	2.8164(9)	14.045(0)	7.9989(0)	0.119	6.96
750	2.8160(9)	14.053(4)	–	0.133	7.94
850	2.8163(6)	14.054(3)	–	0.141	9.10
950	2.8162(7)	14.053(0)	–	0.155	10.8

[a] Based on two-phase model for temperatures ≤650 °C and single-phase model for >650 °C.

variation of the cell parameters are at the detecting limit of the instrument, the cell parameters can be considered constant regardless of the annealing temperature. Fig. 5a shows a typical good fit for samples annealed at a high temperature, while Fig. 5b shows a typical poor fit for samples annealed at lower temperatures. The fitting residue in Fig. 5b suggests the existence of a third set of weak diffraction peaks. Therefore, we performed a simple peak deconvolution using a type 2 pseudo-Voigt peak to identify the number of components in area around 5.1° and 16.8°. As a reference, the HRXRD pattern for the sample annealed at 850 °C

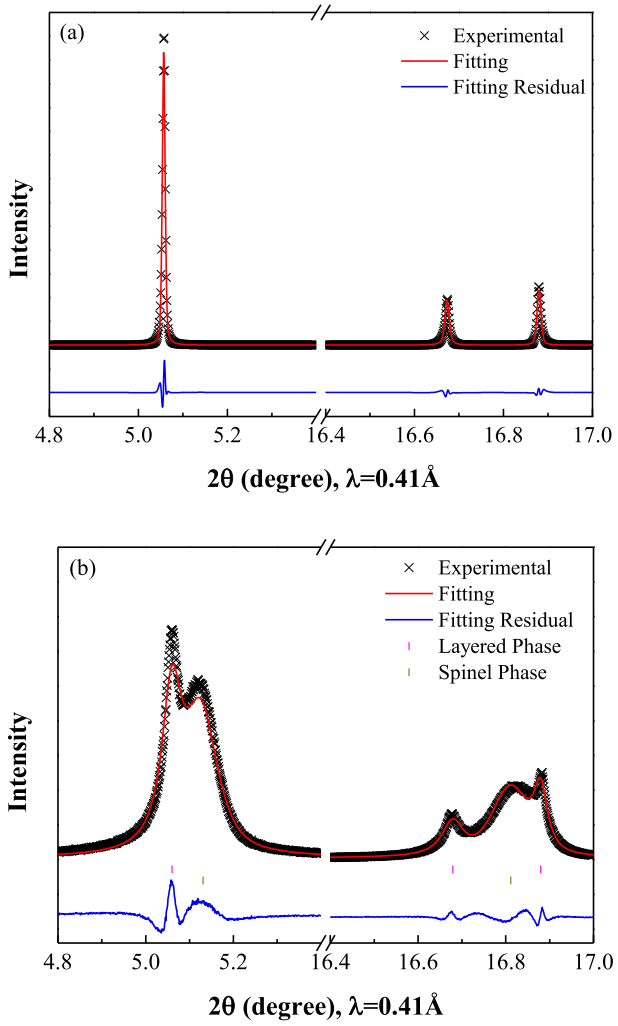

Fig. 5. Typical Rietveld refinement results for materials annealed at (a) 850 °C and (b) 550 °C.

was also included to help in peak assignment. The diffraction data in the 2θ window between 4.8° and 5.3° were successfully decomposed into three independent peaks, whose peak positions remained constant regardless of the annealing temperature (left panel in Fig. 6). We assigned the sharp peak at the left to the $(003)_L$ peak of layered $LiCoO_2$, the right peak at about 5.15° to the $(111)_S$ peak of the spinel $Li_2Co_2O_4$, and the broad, weak peak in the middle to the $(111)_{S'}$ peak of a strained spinel phase. The diffraction data in the 2θ window between 16.5° and 17.0° were deconvoluted into four peaks (right panel in Fig. 6). The $(107)_L$ and $(110)_L$ peaks for layered $LiCoO_2$ were assigned to two sharp peaks at 16.63° and 16.88°, respectively. The one at 16.82° was assigned to the $(551)_S$ peak of the spinel $Li_2Co_2O_4$. Similar to the results shown in the left panel of Fig. 6, a broad, low intensity peak was identified (at about 16.74°). In general, layered $LiCoO_2$ deviates from the standard cubic spinel structure ($c/a = 2\sqrt{6}$), leading to the splitting between the $(107)_L$ and $(110)_L$ peaks. Hence, the minor phase is more likely a spinel phase due to the lack of another peak. In addition, the minor phase should have a crystal structure between the layered and the spinel structures based on the relative peak positions. More than likely, the minor phase was a strained spinel phase that bridged the crystalline $LiCoO_2$ and $Li_2Co_2O_4$.

Half cells using the cathode materials annealed at 450–950 °C were cycled between 3.0 V and 4.2 V vs. Li^+/Li for two cycles. Fig. 7 shows the voltage profiles of these cells, and the corresponding differential capacity profiles (dQ/dV) are plotted in Fig. 8. For the materials annealed at 750 °C and above, the cells delivered a high reversible specific capacity of 141 mAh g^{-1} with a small potential hysteresis between the charge and discharge profiles (see Fig. 7d–f). The pair of sharp dQ/dV peaks at about 3.9 V vs. Li^+/Li was assigned to the redox reaction between $LiCoO_2$ and $Li_{0.5}CoO_2$ (see Fig. 8d–f). When the materials were annealed at 650 °C and below, we observed a huge initial irreversible capacity loss (IICL), which decreased dramatically with the annealing temperature (Fig. 7a–c). After the initial cycle, the cells still retained small portion of their initial capacity; the dQ/dV profiles of the second cycle agreed well with that of the redox reaction between $LiCoO_2$ and $Li_{0.5}CoO_2$ (Fig. 8a–c). The potential hysteresis for the cathode materials annealed at low temperatures was substantially greater than that of materials annealed at high temperatures. As evidenced from both the electrochemical and the HRXRD data (Fig. 4), the potential hysteresis and the large IICL were caused by the existence of the spinel $Li_2Co_2O_4$.

Fig. 9 shows a strong linear relationship between the discharge capacities of the cathode materials treated at different annealing temperatures and their initial charge capacities. Assuming that the samples were physical mixtures of two independent phases and taking into consideration that $LiCoO_2$ has a very small IICL and $Li_2Co_2O_4$ a large IICL, one can easily predict the linear relationship shown in Fig. 9, as well as a large IICL of about 80 mAh g^{-1} for $Li_2Co_2O_4$. This two-phase model also predicts that the samples annealed at 750 °C and above would be mostly $LiCoO_2$ while the sample annealed at 650 °C would be a mixture of about 70% $LiCoO_2$ and 30% $Li_2Co_2O_4$. If the peak areas of $(003)_L$ and $(111)_S$ are used to estimate the ratio between $LiCoO_2$ and $Li_2Co_2O_4$, the sample annealed at 650 °C is composed of about 95% $LiCoO_2$ and 5% $Li_2Co_2O_4$. This discrepancy indicates that the real mechanism might be more than the simple two-phase mixture.

Fig. 10 schematically shows the atomic ordering in both layered $LiCoO_2$ and spinel $Li_2Co_2O_4$. The serious overlapping of diffraction peaks between $LiCoO_2$ and $Li_2Co_2O_4$ suggests similar spacing between diffraction planes, as shown in Fig. 10. The striking difference between $LiCoO_2$ and $Li_2Co_2O_4$ lies in the systematic Li/Co intermixing in $Li_2Co_2O_4$. In the layered framework, both lithium and cobalt columns line up to form separated lithium and cobalt layers.

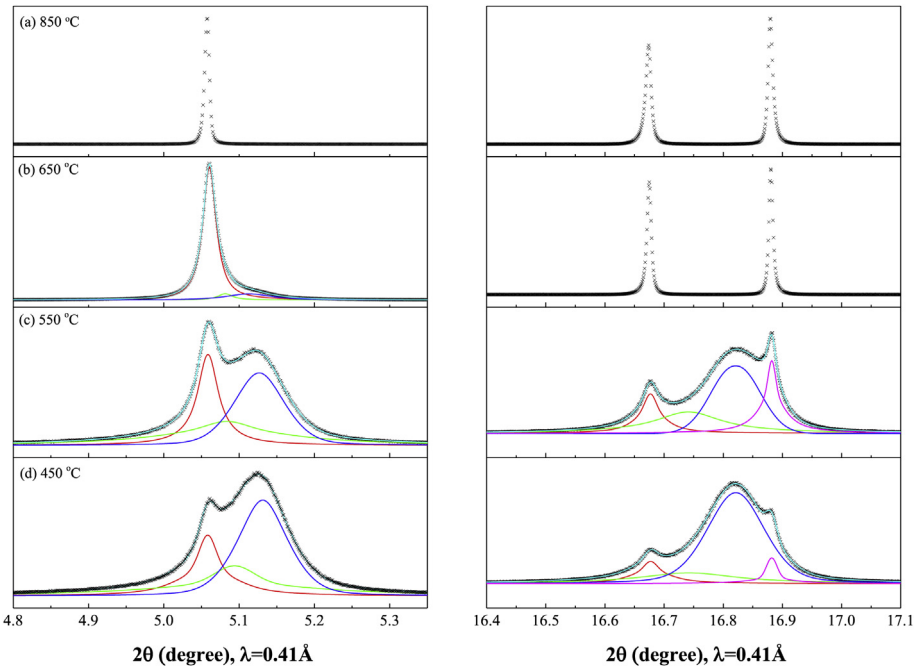

Fig. 6. Peak deconvolution of HRXRD profiles.

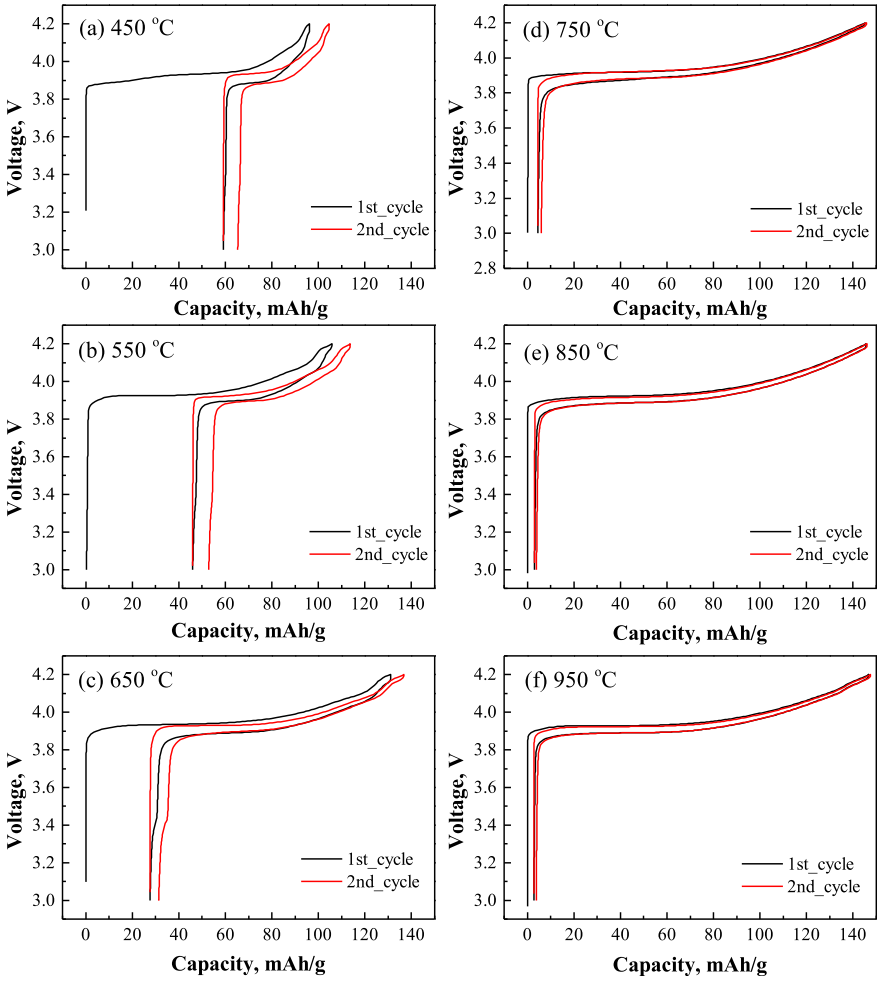

Fig. 7. Voltage profiles of half cells using the cathode materials annealed at different temperature. The cells were cycled between 3.0 V and 4.2 V at a constant current of C/10.

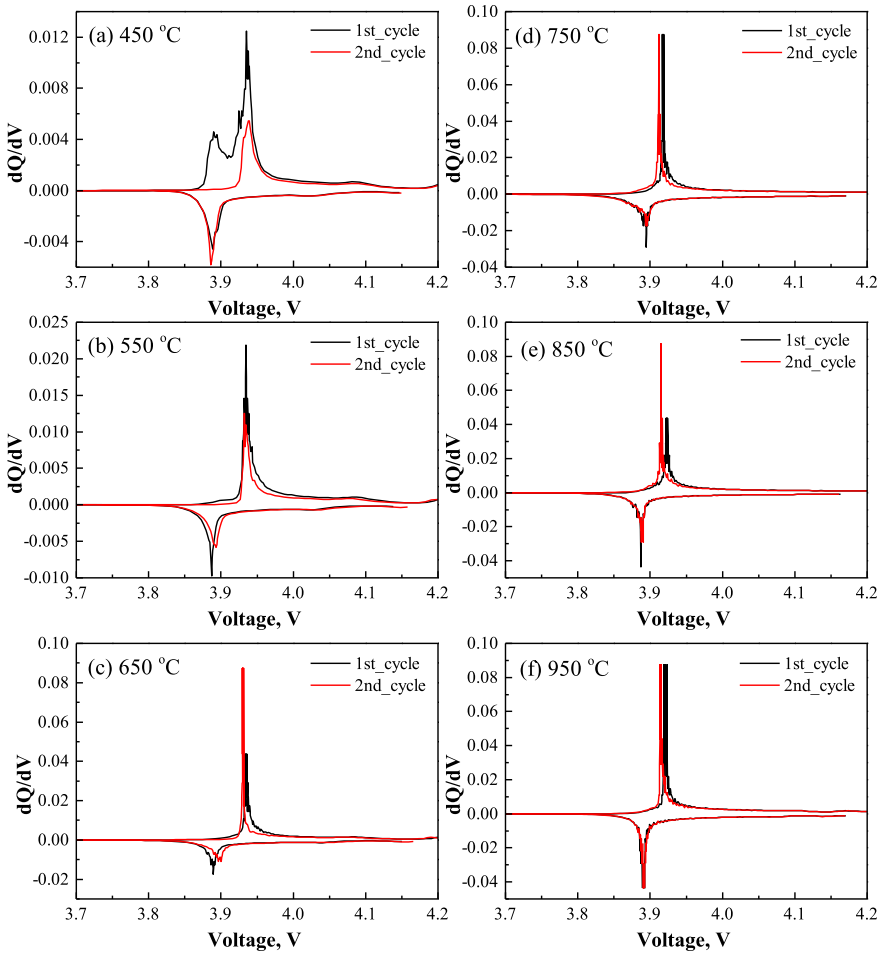

Fig. 8. Differential capacity profiles of half cells whose voltage profiles are shown in Fig. 7.

However, in the $Li_2Co_2O_4$ framework, every other lithium column (or cobalt column) is doped with 50% cobalt (or lithium), resulting in the loss of the lithium diffusion channel. Fig. 10 suggests that the conversion reaction from the spinel $Li_2Co_2O_4$ to the layered $LiCoO_2$ can be accomplished by the Li/Co exchange between adjunct slabs. The *in situ* HEXRD results show that $Li_2Co_2O_4$ was converted to $LiCoO_2$ at elevated temperatures, but $LiCoO_2$ was not converted back to $Li_2Co_2O_4$ during the slow cooling process. This finding indicates that $LiCoO_2$ is the overall stable form within the temperature window explored in this work, and the appearance of the transitional metastable $Li_2Co_2O_4$ originates from the pre-occupation of cobalt atoms in the precursor, spinel Co_3O_4 [14]. The HRXRD profiles in Fig. 4 also show a small mismatch in lattice parameters between the spinel $Li_2Co_2O_4$ and the layered $LiCoO_2$; thus, one can anticipate the existence of an interfacial phase to bridge the $LiCoO_2$ and the $Li_2Co_2O_4$ domain. We believe that this interfacial phase is a strained spinel framework, matching the minor phase shown in Fig. 5; the small dislocation of atoms caused by the strain can also help to reduce the energy barrier for Li/Co exchange. Before the completion of the conversion reaction from $Li_2Co_2O_4$ to $LiCoO_2$, the strained interfacial spinel phase covers the outer boundary of the $LiCoO_2$ domains, acting as a percolation barrier for the lithium diffusion. This leads to the increase of the potential hysteresis (see Fig. 7a–c) and a significant reduction of lithium utilization in the cathode materials annealed at a low temperature, such as 650 °C (see Fig. 9).

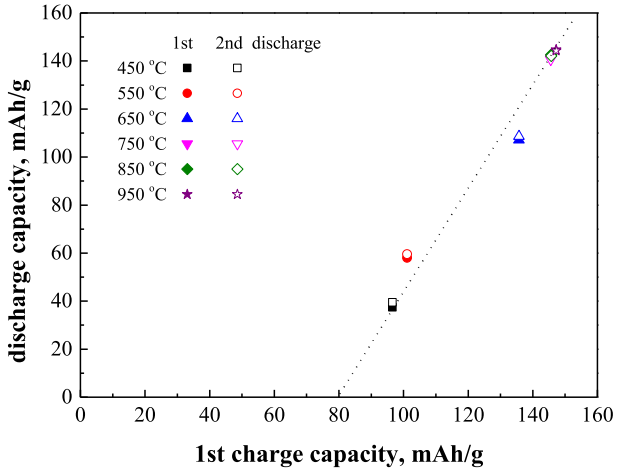

Fig. 9. Discharge capacity versus initial charge capacity for cathode materials with different annealing temperatures.

4. Conclusion

The allotropic structures $LiCoO_2$ and $Li_2Co_2O_4$ are difficult to distinguish using a regular lab-scale X-ray diffractometer. Both *in situ* high-energy X-ray diffraction and *ex situ* high-resolution X-ray diffraction were applied to investigate the formation of $Li_2Co_2O_4$

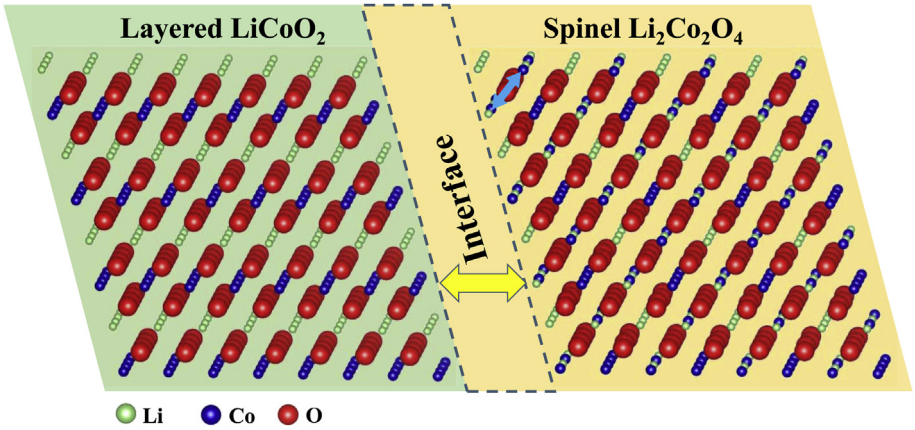

Fig. 10. Schematic showing the conversion mechanism from $Li_2Co_2O_4$ to $LiCoO_2$.

and $LiCoO_2$ during solid-state reaction. Compared to $Li_2Co_2O_4$, layered $LiCoO_2$ is energetically favored, and $Li_2Co_2O_4$ is formed as an intermediate phase during the solid-state synthesis due to the pre-occupation of cobalt atoms in the oxygen framework in the precursor, spinel Co_3O_4. A strained spinel phase was also identified as the interfacial phase, which bridges the layered $LiCoO_2$ and spinel $Li_2Co_2O_4$. It was speculated that the strained spinel phase helps to facilitate Li/Co exchange during the conversion reaction from $Li_2Co_2O_4$ to $LiCoO_2$.

5. Notes

The authors declare no competing financial interest.

Acknowledgment

Research at Argonne National Laboratory was funded by U.S. Department of Energy, Vehicle Technologies Office. Argonne National Laboratory is operated for the U.S. Department of Energy by UChicago Argonne, LLC, under contract DE-AC02-06CH11357. The authors also acknowledge the use of the Advanced Photon Source of Argonne National Laboratory supported by the U.S. Department of Energy, Office of Science, Office of Basic Energy Sciences.

References

[1] J. Berashevich, O. Semeniuk, O. Rubel, J.A. Rowlands, A. Reznik, J. Phys. Condens. Matter *25* (7) (2013) 075803.
[2] P.R. Gao, W.X. Lv, R. Zhang, Y. Liu, G.H. Li, X.F. Bu, L.X. Lei, Methanothermal treatment of carbonated mixtures of $PbSO_4$ and PbO_2 to synthesize alpha-PbO for lead acid batteries, J. Power Sources 248 (2014) 363–369.
[3] M. Comotti, C. Weidenthaler, W.C. Li, F. Schuth, Top. Catal. 44 (1–2) (2007) 275–284.
[4] D. Lee, H.B. Kim, S. Yu, H.J. Kim, W.I. Lee, D.J. Jang, J. Mater. Sci. 49 (9) (2014) 3414–3422.
[5] L. Qin, X.X. Pan, L. Wang, X.P. Sun, G.L. Zhang, X.W. Guo, Appl. Catal. B 150 (2014) 544–553.
[6] V.F. Silva, V. Bouquet, S. Deputier, S. Boursicot, S. Ollivier, I.T. Weber, V.L. Silva, I.M.G. Santos, M. Guilloux-Viry, A. Perrin, J. Appl. Crystallogr. 43 (2010) 1502–1512.
[7] D.Q. Zhang, M.C. Wen, S.S. Zhang, P.J. Liu, W. Zhu, G.S. Li, H.X. Li, Appl. Catal. B 147 (2014) 610–616.
[8] U.M. Patil, J.S. Sohn, S.B. Kulkarni, H.G. Park, Y. Jung, K.V. Gurav, J.H. Kim, S.C. Jun, Mater. Lett. 119 (2014) 135–139.
[9] M. Yang, Q. Ling, H.X. Yang, C.S. Li, A.M. Zhang, Catal. Commun. 46 (2014) 238–241.
[10] C.L. Yu, G. Li, L.F. Wei, Q.Z. Fan, Q. Shu, J.C. Yu, Catal. Today 224 (2014) 154–162.
[11] C.L. Yuan, Y. Zhang, Y. Pan, X.W. Liu, G.L. Wang, D.X. Cao, Electrochim. Acta 116 (2014) 404–412.
[12] A. Zahoor, H.S. Jang, J.S. Jeong, M. Christy, Y.J. Hwang, K.S. Nahm, RSC Adv. 4 (18) (2014) 8973–8977.
[13] Q.B. Wang, Y.W. Wen, R. Chen, B. Shan, J. Alloys Compd. 586 (2014) 611–615.
[14] S.A. Wicker, E.H. Walker Jr., Inorg. Chem. 52 (4) (2013) 1772–1779.
[15] R.J. Gummow, M.M. Thackeray, W.I.F. David, S. Hull, Mater. Res. Bull. 27 (3) (1992) 327–337.
[16] Y. Shao-Horn, S.A. Hackney, C.S. Johnson, A.J. Kahaian, M.M. Thackeray, J. Solid State Chem. 140 (1) (1998) 116–127.
[17] Y. Shao-Horn, S.A. Hackney, A.J. Kahaian, M.M. Thackeray, J. Solid State Chem. 168 (1) (2002) 60–68.
[18] Y. Shao-Horn, S. Levasseur, F. Weill, C. Delmas, J. Electrochem. Soc. 150 (3) (2003) A366–A373.
[19] Z.H. Chen, Y. Ren, Y. Qin, H.M. Wu, S.Q. Ma, J.G. Ren, X.M. He, Y.K. Sun, K. Amine, J. Mater. Chem. 21 (15) (2011) 5604–5609.